

# In Situ Spectroelectrochemical Investigations of Ru<sup>II</sup> Complexes with Bispyrazolyl Methane Triarylamine Ligands

Carol Hua,<sup>A</sup> Brendan F. Abrahams,<sup>B</sup> Floriana Tuna,<sup>C</sup> David Collison,<sup>C</sup> and Deanna M. D'Alessandro<sup>A,D</sup>

<sup>A</sup>School of Chemistry, The University of Sydney, Sydney, NSW 2006, Australia.

<sup>B</sup>School of Chemistry, The University of Melbourne, Melbourne, Vic. 3010, Australia.

<sup>C</sup>School of Chemistry, The University of Manchester, Manchester, M13 9PL, UK.

<sup>D</sup>Corresponding author. Email: deanna.dalessandro@sydney.edu.au

The synthesis and characterization of two triarylamine ligands, 4-(di(1*H*-pyrazol-1-yl)methyl)-*N*-(4-(di(1*H*-pyrazol-1-yl)methyl)phenyl)-*N*-phenylaniline (TPA-2bpm) and tris(4-(di(1*H*-pyrazol-1-yl)methyl)phenyl)amine (TPA-3bpm), containing the bispyrazolylmethane moiety and its Ru<sup>II</sup> terpyridine complexes are presented. The redox properties of the ligands and Ru<sup>II</sup> complexes are explored in detail through cyclic and square-wave voltammetry in addition to in situ UV-vis-near infrared, electron paramagnetic resonance, and fluorescence spectroelectrochemistry. It was demonstrated that the triarylamine radical cation was able to be generated, and further, TPA-2bpm underwent an electrochemically induced dimerization process.

Manuscript received: 30 September 2016.

Manuscript accepted: 15 December 2016.

Published online: 1 February 2017.

## Introduction

The development of materials for applications in optoelectronic devices, dye-sensitized solar cells, and conductive materials is particularly important in the pursuit of technologies for renewable resources. In this regard, ruthenium complexes based on terpyridine and bipyridine ligands have received considerable attention in several areas including water oxidation,<sup>[1]</sup> solar light to energy conversion,<sup>[2–5]</sup> optoelectronic applications,<sup>[6,7]</sup> and catalysis.<sup>[8,9]</sup> The family of coordination compounds derived from 2,2'-bipyridine (bpy), [Ru<sup>II</sup>(bpy)<sub>3</sub>]<sup>2+</sup>, has been widely studied for their charge-transfer properties from excited electronic states, which have applications in solar cells for the conversion of visible radiation into chemical energy.

Several Ru<sup>II</sup> complexes with triarylamine-based ligands have been developed for applications in optoelectronic devices, dye-sensitized solar cells,<sup>[10,11]</sup> and conductive materials. A common motif is the use of either a bipyridine or terpyridine co-ligand in conjunction with a triarylamine-containing ligand.<sup>[10,12]</sup> Triarylamines undergo a one-electron oxidation either by chemical or electrochemical means to form their radical cation state. When two or more triarylamines are covalently linked via a bridge facilitating electronic coupling, mixed-valence systems result.<sup>[13–19]</sup> The redox centres are transformed into different formal oxidation states by the removal of an electron, creating a 'hole' in the system, which may be localized on one of the redox centres, or if the two redox centres are strongly coupled, may be symmetrically delocalized onto several sites.<sup>[19–22]</sup> Mixed-valence compounds, in addition to being valuable systems for the understanding of electron transfer, have significant potential for use in molecular

electronics,<sup>[23]</sup> photovoltaic devices, and dye-sensitized solar cells.<sup>[24–26]</sup>

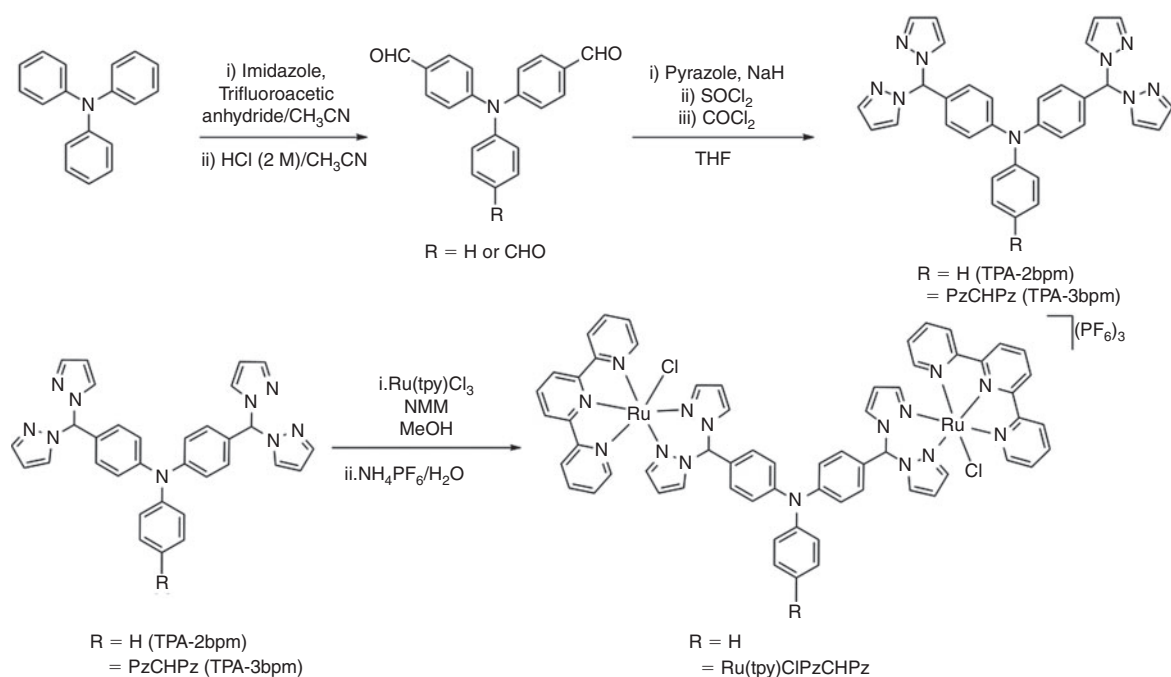
In the current work, we present the synthesis and characterization of two novel triarylamine bispyrazolyl methane ligands, tris(4-(di(1*H*-pyrazol-1-yl)methyl)phenyl)amine (TPA-3bpm) and 4-(di(1*H*-pyrazol-1-yl)methyl)-*N*-(4-(di(1*H*-pyrazol-1-yl)methyl)phenyl)-*N*-phenylaniline (TPA-2bpm), and their resulting Ru<sup>II</sup> terpyridine complexes. The redox properties of the ligands and Ru<sup>II</sup> complexes are examined in detail through cyclic and square-wave voltammetries in addition to in situ UV-vis-near infrared, electron paramagnetic resonance (EPR), and fluorescence spectroelectrochemistry. The presence of an electrochemically induced dimerization process of the TPA-2bpm ligand is also discussed.

## Results and Discussion

### Synthesis and Characterization

The ligands 4-(di(1*H*-pyrazol-1-yl)methyl)-*N*-(4-(di(1*H*-pyrazol-1-yl)methyl)phenyl)-*N*-phenylaniline (TPA-2bpm) and tris(4-(di(1*H*-pyrazol-1-yl)methyl)phenyl)amine (TPA-3bpm) were synthesized via a two-step reaction (Scheme 1) involving formylation of triphenylamine followed by a cobalt condensation with pyrazole to yield TPA-2bpm as a cream solid (68 % yield) and TPA-3bpm as a pale yellow solid (65 % yield).

Colourless block crystals of TPA-2bpm and TPA-3bpm were obtained on slow evaporation of solvent from a solution of the ligand in chloroform (TPA-2bpm) or vapour diffusion of pentane into a solution of the ligand in dichloromethane (TPA-3bpm). The structure of TPA-2bpm was solved and



**Scheme 1.** Synthesis of TPA-2bpm and TPA-3bpm ligands (top), and Ru<sup>II</sup> terpyridine complexes (bottom). CH<sub>3</sub>CN = acetonitrile; THF = tetrahydrofuran; tpy = 2,6-bis(2-pyridyl)pyridine, more commonly referred to as terpyridine; NMM = *N*-methylmorphine; MeOH = methanol.

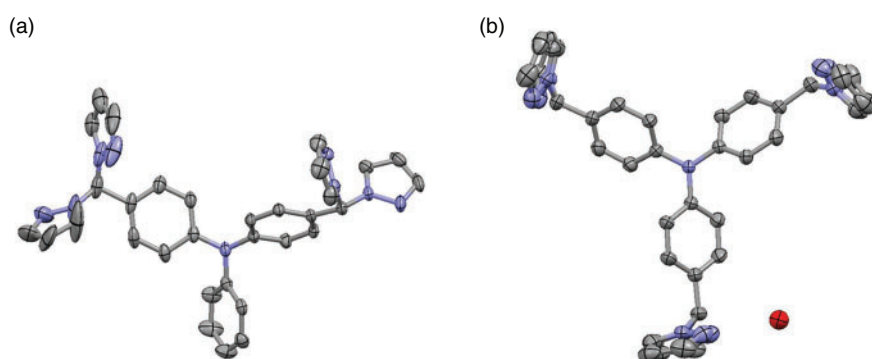


**Fig. 1.** Crystal structure of the (a) TPA-2bpm ligand showing the asymmetric unit; and (b) TPA-3bpm ligand (only a single component of the disordered structure is shown) at 50% thermal ellipsoids where the hydrogens have been omitted for clarity; C, grey; N, blue; O, red.

refined in the triclinic space group *P*-1. The asymmetric unit consisted of one ligand unit where the nitrogen binding sites in the bispyrazolylmethane (bpm) moiety point away from each other (Fig. 1a). The large thermal ellipsoids of the atoms of the pyrazole rings suggest rotational movement of the ring about the methine linkage that joins the two pyrazole rings. The crystal structure of TPA-3bpm was solved and refined in the hexagonal space group *P*6<sub>3</sub>/*m* where the asymmetric unit consisted of one sixth of a TPA-3bpm ligand with an associated water molecule (Fig. 1b). The pyrazole and phenyl rings are both disordered over two positions.

Ruthenium complexes with the TPA-2bpm and TPA-3bpm ligands were synthesized by heating the ligand with Ru(tpy)Cl<sub>3</sub> (tpy = 2,6-bis(2-pyridyl)pyridine, more commonly referred to as terpyridine) and *N*-methylmorphine (NMM) in dry methanol at reflux. After ion exchange with KPF<sub>6</sub>, dark purple solids were isolated and purified by column chromatography. When the TPA-2bpm ligand was used, [Ru<sub>2</sub>Cl<sub>2</sub>(tpy)<sub>2</sub>(TPA-2bpm)](PF<sub>6</sub>)<sub>2</sub> was isolated in 26% yield while the dark purple monosubstituted

product, [RuCl(tpy)(TPA-2bpm)]PF<sub>6</sub>, was obtained in 6% yield. The <sup>1</sup>H NMR spectrum of [Ru<sub>2</sub>Cl<sub>2</sub>(tpy)<sub>2</sub>(TPA-2bpm)](PF<sub>6</sub>)<sub>2</sub> clearly displayed the presence of both the terpyridine and TPA-2bpm ligands. A loss of symmetry of the terpyridine ligand with unique resonances for each proton in the ligand was observed due to the asymmetric environment about the Ru centre. Assignments for each of the proton resonances were achieved with the aid of a 2D <sup>1</sup>H–<sup>1</sup>H COSY (correlation spectroscopy) NMR experiment.

In the synthesis of the ruthenium complexes with TPA-3bpm, three different species, the mono-, di-, and trisubstituted dark purple ruthenium complexes, were obtained after column chromatography (Supplementary Material). When a reaction time of 20 h was used, the disubstituted species [Ru<sub>2</sub>Cl<sub>2</sub>(tpy)<sub>2</sub>(TPA-3bpm)](PF<sub>6</sub>)<sub>2</sub> was obtained in 45% yield and the trisubstituted species [Ru<sub>3</sub>Cl<sub>3</sub>(tpy)<sub>3</sub>(TPA-3bpm)](PF<sub>6</sub>)<sub>3</sub> in 47% yield with a small quantity (<5%) of the monosubstituted [RuCl(tpy)(TPA-3bpm)]PF<sub>6</sub> species. A larger quantity of the [RuCl(tpy)(TPA-3bpm)]PF<sub>6</sub> complex could be obtained with a

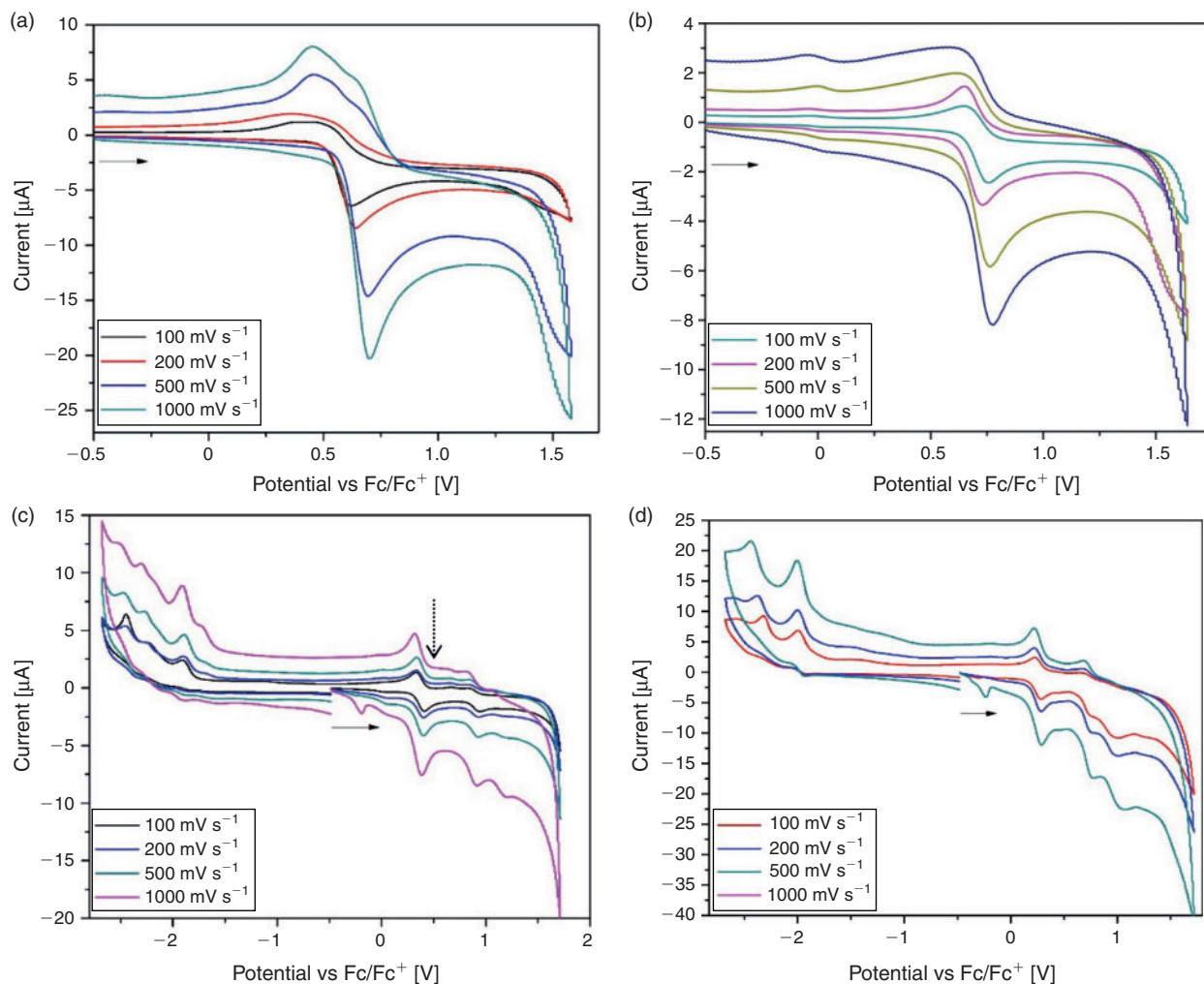


**Fig. 2.** Cyclic voltammograms of (a) TPA-2bpm; (b) TPA-3bpm; (c)  $[\text{Ru}_2\text{Cl}_2(\text{tpy})_2(\text{TPA-2bpm})](\text{PF}_6)_2$ ; and (d)  $[\text{RuCl}(\text{tpy})(\text{TPA-3bpm})]\text{PF}_6$  at scan rates of 100–1000  $\text{mV s}^{-1}$  in  $[(n\text{-C}_4\text{H}_9)_4\text{N}]\text{PF}_6/\text{CH}_3\text{CN}$  electrolyte referenced against the  $\text{Fc}/\text{Fc}^+$  couple where the solid arrow indicates the direction of the forward scan. The dashed arrow at  $\sim 0.6$  V in (c) indicates the peak in the reverse cycle that is indicative of an electrochemical–chemical (EC) process.

shorter reaction time of 4 h. The  $^1\text{H}$  NMR spectrum of the  $[\text{Ru}_3\text{Cl}_3(\text{tpy})_3(\text{TPA-3bpm})](\text{PF}_6)_3$  complex was complicated, with the symmetry of the complex being split around the terpyridine resonances, resulting in different chemical shifts for the three terpyridine groups coordinated to the three ruthenium centres, in addition to the chemically distinct environments for the ligand resonances. The correct mass at  $m/z$  597.47 corresponding to the triply charged  $[\text{M} - 3\text{PF}_6]^{3+}$  ion (calculated  $m/z$  597.73) was observed by electrospray ionisation mass spectrometry (ESI-MS), confirming the formation of the ruthenium complex.

#### Redox Properties

The redox properties of TPA-2bpm and TPA-3bpm were investigated using cyclic voltammetry experiments in  $[(n\text{-C}_4\text{H}_9)_4\text{N}]\text{PF}_6/\text{CH}_3\text{CN}$  and  $[(n\text{-C}_4\text{H}_9)_4\text{N}]\text{PF}_6/\text{CH}_2\text{Cl}_2$  electrolytes at scan rates of 10–1000  $\text{mV s}^{-1}$  (Fig. 2 and Supplementary Material). One quasi-reversible peak was observed for TPA-2bpm and TPA-3bpm at  $\sim 0.6$  V versus ferrocene ( $\text{Fc}/\text{Fc}^+$ ) in both electrolytes, which was attributed to the one-electron oxidation of the triarylamine core to its radical cation.

The peak at  $\sim 0.6$  V for TPA-2bpm became increasingly irreversible and exhibited a shift to higher potentials on

performing multiple cycling experiments in  $[(n\text{-C}_4\text{H}_9)_4\text{N}]\text{PF}_6/\text{CH}_2\text{Cl}_2$  owing to dimerization through the *para* position of the TPA-2bpm ligand, which is a well-known phenomenon for triaryl amines (see Supplementary Material).<sup>[27,28]</sup> The presence of an electrochemical–chemical (EC) process was supported by the irreversibility of the oxidative process for TPA-2bpm at low scan rates (10–50  $\text{mV s}^{-1}$ ), but increasing reversibility at fast scan rates (100–1000  $\text{mV s}^{-1}$ ) when there is insufficient time for dimerization to occur (Fig. 2 and Supplementary Material). The dimerization of the ligand was accelerated in less polar solvents such as dichloromethane, where the cyclic voltammogram over the range of scan rates from 100 to 1000  $\text{mV s}^{-1}$  displayed a more irreversible process than in acetonitrile, which is in accordance with previously reported trends (Supplementary Material).<sup>[29]</sup> As expected, TPA-3bpm showed no evidence for dimerization, with the peak due to formation of the triarylamine radical cation remaining reversible over a range of scan rates and electrolytes (Supplementary Material).

Two main anodic processes were observed for all ruthenium complexes, where the reversible process at  $\sim 0.4$  V versus  $\text{Fc}/\text{Fc}^+$  was assigned to the one-electron oxidation of  $\text{Ru}^{\text{II}}$  to  $\text{Ru}^{\text{III}}$  (Fig. 2c, d, Supplementary Material); the quasi-reversible second process at  $\sim 0.9$  V versus  $\text{Fc}/\text{Fc}^+$  was due to the one-electron oxidation of

the triarylamine to its radical cation state. Several irreversible processes occur in the cathodic region due to reduction of the terpyridine ligand.

In the cyclic voltammogram of  $[\text{Ru}_2\text{Cl}_2(\text{tpy})_2(\text{TPA-2bpm})](\text{PF}_6)_2$ , a second peak was observed on the reverse cycle at  $\sim 0.6$  V versus  $\text{Fc}/\text{Fc}^+$ , which suggested that an EC process was occurring during the forward sweep (Fig. 2c). The irreversible EC process became increasingly prominent at fast scan rates of 500 and 1000  $\text{mV s}^{-1}$  and may be attributed to dimerization of TPA-2bpm as observed in the electrochemical and spectroelectrochemical experiments (see above) for the ligand.

Electrochemical experiments on the  $\text{Ru}^{\text{II}}$ -containing TPA-3bpm complexes displayed more complex behaviour than those containing TPA-2bpm with regards to the oxidation of the triarylamine core (Fig. 2d, Supplementary Material). In  $[\text{RuCl}(\text{tpy})(\text{TPA-3bpm})]\text{PF}_6$ , the additional process at  $\sim 0.75$  V versus  $\text{Fc}/\text{Fc}^+$  may indicate electronic communication between the oxidized  $\text{Ru}^{\text{III}}$  centre and the triarylamine core. As expected, the complexes containing TPA-3bpm were highly stable on electrochemical cycling between  $-0.6$  and  $1.75$  V versus  $\text{Fc}/\text{Fc}^+$  at  $100 \text{ mV s}^{-1}$  (see Supplementary Material).

#### UV-Vis-Near IR Spectroelectrochemistry

A UV-vis-NIR spectroelectrochemical experiment on TPA-2bpm revealed four new bands at 7600, 14300, 20600, and 28100  $\text{cm}^{-1}$  on application of a positive potential (of 0.9 V),

while the band at 32800  $\text{cm}^{-1}$  decreased (Fig. 3). The bands appearing at 14300 and 28100  $\text{cm}^{-1}$  can be assigned to oxidation of the triarylamine core to its radical cation state and are consistent with previously reported triarylamine systems.<sup>[14,30]</sup> The bands at 7600 and 20600  $\text{cm}^{-1}$  indicate dimerization of the ligand at the unsubstituted *para* position, where the appearance of the band in the NIR region was indicative of the formation of a mixed-valence state and associated intervalence charge-transfer process. The dimerization of triarylamines with unsubstituted *para* positions on oxidation has been proposed to proceed owing to the coupling of two molecules containing radical species located on the *para* position of the phenyl ring (see Supplementary Material).<sup>[15,28,29]</sup> The dimerization leads to a short distance (9.9 Å) between adjacent triarylamine cores, allowing electronic communication to occur via a low-energy electron-transfer pathway.<sup>[14]</sup> As the potential applied to TPA-2bpm was increased from 1.0 to 1.2 V, the adjacent triarylamine core was oxidized to its radical cation, leading to a decrease in the intensity of the NIR band at 7600  $\text{cm}^{-1}$ .

The solution-state spectroelectrochemical experiment for TPA-3bpm in  $[(n\text{-C}_4\text{H}_9)_4\text{N}]\text{PF}_6/\text{CH}_3\text{CN}$  electrolyte was characterized by the formation of bands at 14400 and 27500  $\text{cm}^{-1}$  and a decrease in the band at 32300  $\text{cm}^{-1}$ , which can be attributed to the one-electron oxidation of the triarylamine core to its corresponding radical cation state (see Supplementary Material). Bands at 7600 and 20600  $\text{cm}^{-1}$  (as observed for TPA-2bpm) were not formed as all *para* positions on the triarylamine

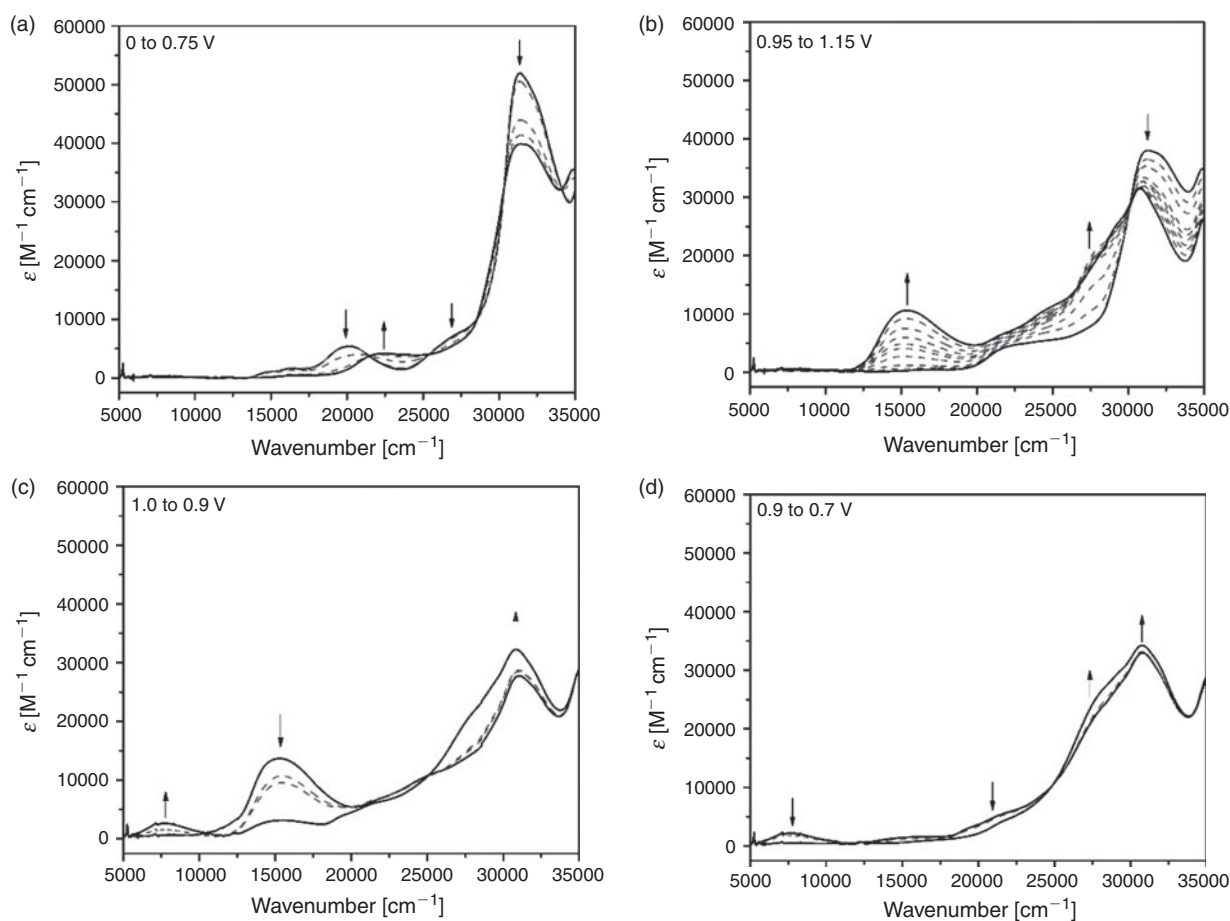


**Fig. 3.** Solution state UV-vis-NIR spectroelectrochemistry of  $[\text{Ru}_2\text{Cl}_2(\text{tpy})_2(\text{TPA-2bpm})](\text{PF}_6)_2$  in  $[(n\text{-C}_4\text{H}_9)_4\text{N}]\text{PF}_6/\text{CH}_3\text{CN}$  electrolyte where the potential was increased from (a) 0 to 0.75 V; (b) 0.95 to 1.15 V; and decreased from (c) 1.0 to 0.9 V; and (d) 0.9 to 0.7 V. The dashed lines represent the intermediate spectra obtained over each potential range.

ligand are substituted in the TPA-3bpm ligand, precluding any dimerization process.

All ruthenium complexes displayed similar spectral properties and trends in the spectral responses during oxidation. In the neutral state, there are two main bands at  $\sim 20000$  and  $30000\text{ cm}^{-1}$  (Fig. 3 and Supplementary Material). The band at  $\sim 20000\text{ cm}^{-1}$  was assigned to the  $d \rightarrow \pi^*$  metal-to-ligand charge transfer (MLCT) transition from the  $\text{Ru}^{\text{II}}$  metal centre to the terpyridine ligand, while the band at  $30000\text{ cm}^{-1}$  was due to the  $\pi \rightarrow \pi^*$  transitions of the aromatic systems present.

On application of a potential of  $0.75\text{ V}$  to all ruthenium complexes, the MLCT transition exhibited a blue shift from  $\sim 20000$  to  $\sim 22000\text{ cm}^{-1}$  due to oxidation of the  $\text{Ru}^{\text{II}}$  centre to  $\text{Ru}^{\text{III}}$ . The second process involved the formation of a band at  $\sim 15000\text{ cm}^{-1}$  due to the localized  $\pi \rightarrow \pi^*$  transition of the triarylamine radical cation in the ligand. The third process for all ruthenium complexes except  $[\text{Ru}_2\text{Cl}_2(\text{tpy})_2(\text{TPA-2bpm})](\text{PF}_6)_2$  involved a decrease in the intensities of the bands at  $\sim 15000$  and  $26500\text{ cm}^{-1}$  due to decomposition of the complex. Interestingly, for  $[\text{Ru}_2\text{Cl}_2(\text{tpy})_2(\text{TPA-2bpm})](\text{PF}_6)_2$ , a band in the NIR region at  $7740\text{ cm}^{-1}$  was formed as the potential was decreased from  $1.0$  to  $0.9\text{ V}$ , which was indicative of an intervalence charge transfer (IVCT) process and strongly suggests dimerization of the complex through the unsubstituted *para* position on the triarylamine core (Fig. 3). As the potential was decreased from  $0.9$  to  $0.7\text{ V}$ , the bands at  $7740$  and  $\sim 15000\text{ cm}^{-1}$  decreased in intensity to reveal a spectrum that was similar to the starting neutral spectrum.

#### Intervalence Charge Transfer

Analysis of the Gaussian-shaped IVCT bands in the NIR region formed in the solution-state spectroelectrochemical spectra of the TPA-2bpm ligand and  $[\text{Ru}_2\text{Cl}_2(\text{tpy})_2(\text{TPA-2bpm})](\text{PF}_6)_2$  complex due to dimerization was undertaken to determine the extent of charge delocalization (Supplementary Material). TPA-2bpm exhibits a band centred at  $7582\text{ cm}^{-1}$  ( $\nu_{\text{max}}$ ) with an associated extinction coefficient ( $\epsilon_{\text{max}}$ ) of  $881\text{ M}^{-1}\text{ cm}^{-1}$ .

Comparison of the linewidth of the band at half height ( $\Delta\nu_{1/2}$ ) of  $3325\text{ cm}^{-1}$  with the theoretical value calculated from the classical theory of Hush<sup>[31,32]</sup> ( $\Delta\nu_{1/2}^\circ$ ) of  $4185\text{ cm}^{-1}$  suggests that the system is characteristic of a localized mixed-valence compound. Further support can be found through comparison of the electronic matrix coupling element,  $H_{\text{ab}}$ , where  $2H_{\text{ab}}$  provides a measure of the difference between the lower and upper potential energy surfaces (details of the calculation are provided in the Supplementary Material).<sup>[21]</sup> For TPA-2bpm, the value of  $2H_{\text{ab}}$  ( $674\text{ cm}^{-1}$ ) is significantly smaller than  $\nu_{\text{max}}$  ( $7582\text{ cm}^{-1}$ ), confirming that the IVCT transition is localized and therefore can be described as a Class II system in the Robin and Day classification.<sup>[33]</sup>

The  $[\text{Ru}_2\text{Cl}_2(\text{tpy})_2(\text{TPA-2bpm})](\text{PF}_6)_2$  complex was also determined to be a localized mixed-valence class II system on analysis of the band at  $\nu_{\text{max}} 7783\text{ cm}^{-1}$  ( $\epsilon_{\text{max}} 2620\text{ M}^{-1}\text{ cm}^{-1}$ ) with a comparison of the line width at half height,  $\Delta\nu_{1/2} = 3495\text{ cm}^{-1}$  with the theoretically calculated value,  $\Delta\nu_{1/2}^\circ = 4240\text{ cm}^{-1}$ . The value of  $2H_{\text{ab}}$  in this system,  $1131.5\text{ cm}^{-1}$ , which is higher than that for the TPA-2bpm ligand suggests that although this system is still a class II compound, the two centres are more strongly coupled in the Ru complex than in the ligand. The IVCT bands in both TPA-2bpm and  $[\text{Ru}_2\text{Cl}_2(\text{tpy})_2(\text{TPA-2bpm})](\text{PF}_6)_2$  exhibit a small cut-off on the low-energy side of the band, resulting in a slightly asymmetric Gaussian band. This is characteristic of coupled systems where the Gaussian shape of the band is retained, but is truncated at energies below the value of  $2H_{\text{ab}}$ .<sup>[21]</sup>

#### EPR Spectroelectrochemistry

Application of a potential of  $1.7\text{ V}$  during the EPR spectroelectrochemical experiment for TPA-2bpm in  $[(n\text{-C}_4\text{H}_9)_4\text{N}]\text{PF}_6/\text{CH}_2\text{Cl}_2$  electrolyte resulted in a colourless to a deep orange-red solution (Fig. 4). The radical was readily generated and exhibited a very strong EPR signal at  $g = 2.0046$  ( $g$  indicates the  $g$ -factor, which is  $2.0023$  for the free electron). On simulation of the EPR spectrum, it was revealed

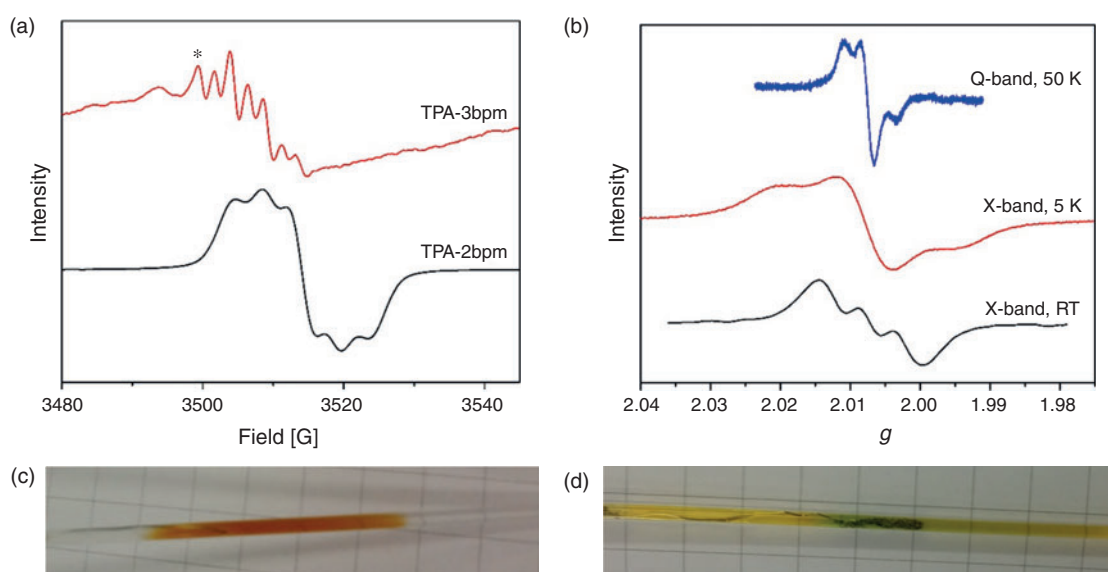


**Fig. 4.** EPR spectroelectrochemistry in  $[(n\text{-C}_4\text{H}_9)_4\text{N}]\text{PF}_6/\text{CH}_2\text{Cl}_2$  electrolyte of (a) TPA-2bpm and TPA-3bpm at room temperature (RT,  $298\text{ K}$ ) in solution at X-Band at a potential of  $1.7\text{ V}$  (\* indicates an impurity); (b)  $[\text{Ru}(\text{tpy})\text{Cl}(\text{TPA-3bpm})]\text{PF}_6$  in  $[(n\text{-C}_4\text{H}_9)_4\text{N}]\text{PF}_6/\text{CH}_3\text{CN}$  electrolyte showing the spectrum of the radical in solution at RT of  $298\text{ K}$  at X-band, as a frozen solution at  $5\text{ K}$  at X-band and as a frozen solution at  $50\text{ K}$  at Q-band; and photos during the experiment of (c) TPA-2bpm; and (d) TPA-3bpm.

that the signal arose from interaction of the radical with two nitrogen nuclei, each exhibiting a hyperfine coupling value of 11.5 MHz (Supplementary Material). The signal was very similar to that reported by Kattnig et al. for a system containing two linked triarylamine cores through a phenyl–ethynyl linker.<sup>[34]</sup> This, along with the previous observations from solution-state electrochemical and UV-vis-NIR spectroelectrochemical experiments strongly supported the formation of a dimer species on oxidation of the triarylamine through the unsubstituted *para* position on the phenyl ring.

As a potential of 1.7 V was applied to a solution of TPA-3bpm in  $[(n\text{-C}_4\text{H}_9)_4\text{N}]\text{PF}_6/\text{CH}_2\text{Cl}_2$  electrolyte, a colour change from yellow to deep green occurred with the appearance of an EPR signal. A distinct lack of dimer formation for TPA-3bpm was observed where the EPR signal ( $g = 2.008$ ) indicated that the radical only interacted with one nitrogen nucleus (the isotropic component of the hyperfine interaction,  $A_{\text{iso}} = 12.6$  MHz) at the centre of the triarylamine ligand in addition to a hyperfine coupling interaction of 5.6 MHz due to the protons that are proximal to the central nitrogen (Fig. 4a). The EPR spectrum of the electrochemically generated radical of TPA-3bpm was additionally obtained as a frozen solution (Supplementary Material). As the temperature was lowered from 200 to 170 K, a gradual transition from the solution-state to solid-state spectrum was observed (Supplementary Material). The solid-state spectrum exhibits rhombic anisotropy, clearly displaying contributions from the  $x$ ,  $y$ , and  $z$  axes (Supplementary Material). The frozen-solution spectrum of TPA-3bpm was determined to have  $g$ -factor values for N of  $g_x = 1.997$ ,  $g_y = 2.007$ ,  $g_z = 2.017$ , and  $A = 2.8$  MHz in addition to a contribution from the  $^1\text{H}$  present in the ligand of  $g = 2.0067$  and  $A = 11.8$  MHz.

EPR spectroelectrochemistry for the ruthenium complexes with the TPA-2bpm ligand revealed a very broad EPR signal on application of a positive potential ( $g = 2.0065$  for  $[\text{Ru}(\text{tpy})\text{Cl}(\text{TPA-2bpm})](\text{PF}_6)$  and  $g = 2.007$  for  $[\text{Ru}_2(\text{tpy})_2\text{Cl}_2(\text{TPA-2bpm})](\text{PF}_6)_2$ ) with minimal hyperfine coupling (Supplementary Material). The hyperfine information was hidden by the line width of the signal, which likely arose from the slow rate of molecular tumbling of the complex in solution. A slight colour change from dark purple to light purple–yellow was observed when the positive potential was first applied to all Ru complexes, corresponding to oxidation of  $\text{Ru}^{\text{II}}$  to  $\text{Ru}^{\text{III}}$ . As the experiment progressed, the light colour generated was replaced by a very dark green–purple corresponding to generation of the triarylamine radical cation. The  $\text{Ru}^{\text{III}}$  species was not able to be observed for  $[\text{Ru}(\text{tpy})\text{Cl}(\text{TPA-2bpm})](\text{PF}_6)$  and  $[\text{Ru}_2(\text{tpy})_2\text{Cl}_2(\text{TPA-2bpm})](\text{PF}_6)_2$  at 130 K owing to the low concentration of the species in addition to the broadening of the signals typical of metal ions.

The EPR signal generated for ruthenium complexes containing the TPA-3bpm ligand contained the distinctive 1 : 1 : 1 triplet signal for a radical localized on a nitrogen atom (Fig. 4b). The elucidation of hyperfine information was possible owing to the different rate of molecular tumbling in solution, as complexes containing TPA-3bpm are significantly different in size and shape from the TPA-2bpm complexes. All complexes exhibited similar  $g$ -factor values, where a slight increase in the  $g$  value was observed as more ruthenium centres were coordinated to the ligand (Supplementary Material). The frozen-solution EPR spectrum for  $[\text{Ru}(\text{tpy})\text{Cl}(\text{TPA-3bpm})]\text{PF}_6$  was obtained at X- and Q-band frequencies to elucidate the small  $g$  anisotropy present (Fig. 4 and Supplementary Material). There was a significant contribution from  $^1\text{H}$  in the ligand to the EPR signal

indicating that the radical generated was delocalized onto the phenyl rings. The EPR signal due to  $\text{Ru}^{\text{III}}$  formed on oxidation was observed at 5 K at X-band and displayed axial anisotropy (Supplementary Material) in addition to the presence of the triarylamine radical cation (Fig. 4b).

### Fluorescence

A fluorescence emission peak was observed for TPA-2bpm (375 nm) and TPA-3bpm (368 nm) on excitation of a solution of the ligand in acetonitrile at 350 nm ( $28571\text{ cm}^{-1}$ ) (Supplementary Material). The observed Stokes shifts were 70 and 60 nm respectively for TPA-2bpm and TPA-3bpm. The oxidized TPA-2bpm and TPA-3bpm ligands were fluorescent but exhibited significant red shifts from their neutral states, emitting fluorescence peaks at 463 nm for TPA-2bpm and 472 nm for TPA-3bpm with corresponding Stokes shifts of 89 nm for TPA-2bpm and 101 nm for TPA-3bpm.

The ruthenium complexes with TPA-2bpm emitted a broad fluorescence peak from 400 to 600 nm on excitation at 350 nm (Supplementary Material). The fluorescence peak at 400–600 nm ( $16670\text{--}25000\text{ cm}^{-1}$ ) for  $[\text{Ru}_2(\text{tpy})_2\text{Cl}_2(\text{TPA-3bpm})](\text{PF}_6)_2$  may be resolved into two overlapping peaks. An additional fluorescence peak at 750 nm ( $13330\text{ cm}^{-1}$ ) was observed for both complexes on excitation into the MLCT band at 500 nm that exhibited a very large Stokes shift of 250 nm. Luminescence on excitation into the MLCT band of ruthenium terpyridine complexes is well known and has resulted in their use as oxygen sensors and in biomedical applications.<sup>[35]</sup>

All ruthenium complexes containing the TPA-3bpm ligand exhibited fluorescence with emission bands at 746–750 nm on excitation into the MLCT band ( $\lambda_{\text{ex}} 490\text{--}495\text{ nm}$ ), suggesting that the fluorescence was a property resulting from interaction of the ligand with the ruthenium centre (Supplementary Material). The fluorescence was quenched for all complexes on chemical oxidation with  $\text{NOPF}_6$  owing to oxidation of the triarylamine to its radical cation. This is in accordance with previously observed trends where the fluorescence can be switched off as a function of the redox state.<sup>[36,37]</sup>

### Conclusions

Two novel ligands, TPA-2bpm and TPA-3bpm, containing a redox-active triarylamine core with the bispyrazolylmethane moiety have been developed. Of particular interest was the comparison of the redox properties between TPA-2bpm and TPA-3bpm, where dimerization of TPA-2bpm occurred owing to the unsubstituted *para* position present. Evidence for the dimerization of TPA-2bpm was obtained using spectroelectrochemical experiments, where formation of a low-energy IVCT band (UV-vis-NIR) and the electron delocalization over two chemically equivalent nitrogens (EPR) were observed. This dimerization process was absent in TPA-3bpm where all *para* sites of the phenyl rings are substituted. The combination of the TPA-2bpm and TPA-3bpm ligands with  $\text{Ru}(\text{tpy})\text{Cl}_3$  yielded five  $\text{Ru}^{\text{II}}$  terpyridine complexes with varying numbers of  $\text{Ru}^{\text{II}}$  coordinated to each ligand. The  $\text{Ru}^{\text{II}}$  and the triarylamine core were able to be oxidized at well-separated potentials, allowing investigation of each of the distinct redox states of the complexes. In particular, UV-vis-NIR and EPR spectroelectrochemical experiments revealed that dimerization also occurred in complexes with the TPA-2bpm ligand. The properties of the synthesized  $\text{Ru}^{\text{II}}$  complexes may lead to their use in optoelectronic devices and dye-sensitized solar cells.

## Experimental

### General Considerations

All chemicals and solvents were used as obtained without further purification. Tris(*p*-formylphenyl)amine<sup>[38]</sup> and Ru(tpy)Cl<sub>3</sub><sup>[39,40]</sup> were synthesized according to literature procedures. 4,4'-(Phenylazanediy)l)dibenzaldehyde was synthesized according to literature procedures with modification.<sup>[38]</sup> For experiments requiring dry solvents, acetonitrile was dried over CaH<sub>2</sub> and methanol was dried over magnesium/magnesium methoxide before being distilled under nitrogen. Toluene was obtained from a PuraSolv solvent purification system and stored over activated 4-Å molecular sieves.

Solution-state <sup>1</sup>H and <sup>13</sup>C{<sup>1</sup>H} NMR spectra were recorded on either a Bruker Avance300 or Avance500 spectrometer operating at 300, 500 MHz for <sup>1</sup>H and 75, 125 MHz for <sup>13</sup>C. <sup>1</sup>H and <sup>13</sup>C NMR chemical shifts were referenced internally to residual solvent resonances. Spectra were recorded at 300 K and chemical shifts (δ), with uncertainties of ±0.01 Hz for <sup>1</sup>H and ±0.05 Hz for <sup>13</sup>C, are quoted in ppm. Coupling constants (*J*) are quoted in Hertz. Deuterated solvents were obtained from Cambridge Stable Isotopes and used as received. Mass spectrometry was carried out at the mass spectrometry analysis facility at the University of Sydney on a Finnigan LCQ mass spectrometer. Microanalyses were carried out at the Chemical Analysis Facility – Elemental Analysis Service in the Department of Chemistry and Biomolecular Science at Macquarie University, NSW, Australia.

### Synthesis of Ligands

#### TPA-2bpm

A suspension of NaH (3.65 g, 60% in mineral oil, 91.3 mmol) in dry THF (200 mL) was cooled in a water–ice bath for 30 min before the addition of pyrazole (6.20 g, 91.1 mmol), which yielded bubbling and a clear solution. This was stirred at 0°C for 40 min before the dropwise addition of thionyl chloride (3.30 mL, 45.4 mmol) to yield a thick white suspension. The reaction mixture was then stirred at room temperature for 30 min before anhydrous cobalt(II) chloride (119 mg, 0.917 mmol) and 4,4'-(phenylazanediy)l)dibenzaldehyde (0.750 g, 2.49 mmol) were added to yield a mustard-yellow suspension. This was then heated at reflux for 30 h to yield a pale green suspension before being cooled to room temperature and the solvent removed under vacuum. The residue was dissolved in dichloromethane and washed with water before being dried over magnesium sulfate, filtered, and the solvent removed under vacuum to yield a yellow oil. The crude product was purified by column chromatography on silica (1 : 3 ethyl acetate/hexane, gradient to 1 : 1 ethyl acetate/hexane) (0.907 g, 68%). δ<sub>H</sub> (CDCl<sub>3</sub>, 500 MHz) 7.67 (s, 2H, H5), 7.63 (d, <sup>3</sup>J<sub>H6–H7</sub> 1.2, 4H, H6), 7.54 (d, <sup>3</sup>J<sub>H7–H8</sub> 1.8, 4H, H8), 7.26 (d, <sup>3</sup>J<sub>H10–H11</sub> 8.7, 1H, H11), 7.09 (d, <sup>3</sup>J<sub>H10–H11</sub> 8.0, 2H, H10), 7.08 (t, <sup>3</sup>J<sub>H11–H12</sub> 8.0, 1H, H12), 7.03 (d, <sup>3</sup>J<sub>H2–H3</sub> 8.7, 4H, H3), 6.89 (d, <sup>3</sup>J<sub>H2–H3</sub> 8.7, 4H, H2), 6.33 (br s, 4H, H7). <sup>13</sup>C{<sup>1</sup>H} NMR (CDCl<sub>3</sub>, 125 MHz) 148.3 (C1), 146.8 (C9), 140.9 (C6), 130.2 (C4), 129.8 (C8), 129.7 (C11), 128.8 (C2), 125.8 (C10), 124.5 (C12), 123.5 (C3), 106.7 (C7), 77.7 (C5). Anal. Calc. for C<sub>32</sub>H<sub>27</sub>N<sub>6</sub>: C 71.49, H 5.06, N 23.45. Found: C 71.21, H 4.77, N 23.14%. *m/z* (ESI<sup>+</sup>, CH<sub>3</sub>CN) 560.00 (100%); [M + Na]<sup>+</sup> requires 560.23.

#### TPA-3bpm

A suspension of NaH (3.64 g, 60% in mineral oil, 91.1 mmol) in dry THF (50.0 mL) was cooled in a water–ice

bath for 30 min before the addition of pyrazole (6.20 g, 91.1 mmol), which yielded bubbling and a clear solution. This was stirred at 0°C for 1.5 h before the dropwise addition of thionyl chloride (3.32 mL, 45.5 mmol) to yield a thick white suspension. The reaction mixture was then stirred at room temperature for 30 min before anhydrous cobalt(II) chloride (118 mg, 0.911 mmol) and tris(*p*-formylphenyl)amine (1.00 g, 3.04 mmol) were added to yield a mustard-yellow suspension. This was then heated at reflux for 30 h to yield a pale green suspension before being cooled to room temperature and the solvent removed under vacuum. The residue was dissolved in dichloromethane and washed with water before being dried over magnesium sulfate, filtered, and the solvent removed under vacuum to yield a red solid. The crude product was purified by column chromatography on silica (1 : 1 ethyl acetate/hexane, gradient to 3 : 1 ethyl acetate/hexane) (1.35 g, 65%). δ<sub>H</sub> (CDCl<sub>3</sub>, 500 MHz) 7.67 (s, 3H, H5), 7.62 (d, <sup>3</sup>J<sub>H7–H8</sub> 2.0, 6H, H8), 7.53 (d, <sup>3</sup>J<sub>H6–H7</sub> 2.0, 4H, H6), 7.04 (d, <sup>3</sup>J<sub>H2–H3</sub> 8.5, 6H, H3), 6.89 (d, <sup>3</sup>J<sub>H2–H3</sub> 8.5, 6H, H2), 6.32 (t, <sup>3</sup>J<sub>H7–H6/H8</sub> 2.0, 6H, H7). <sup>13</sup>C{<sup>1</sup>H} NMR (CDCl<sub>3</sub>, 125 MHz) 147.8 (C1), 140.9 (C8), 130.6 (C4), 129.8 (C6), 128.3 (C2), 124.3 (C3), 106.7 (C7), 77.6 (C5). Anal. Calc. for C<sub>39</sub>H<sub>33</sub>N<sub>13</sub>: C 68.51, H 4.86, N 26.63. Found: C 67.57, H 4.80, N 25.46%. *m/z* (ESI<sup>+</sup>, CH<sub>3</sub>CN) 706.07 (100%); [M + Na]<sup>+</sup> requires 706.29.

### Synthesis of Ruthenium Complexes

#### [Ru<sub>2</sub>Cl<sub>2</sub>(tpy)<sub>2</sub>(TPA-2bpm)](PF<sub>6</sub>)<sub>2</sub>

Ru(tpy)Cl<sub>3</sub> (82.0 mg, 0.186 mmol) and TPA-2bpm (50.0 mg, 0.0930 mmol) were suspended in dry methanol (40.0 mL) and *N*-methylmorpholine (1.5 mL) was added. The dark purple suspension was heated at reflux under nitrogen for 22 h to yield a dark solution, then cooled to room temperature. A saturated solution of KPF<sub>6</sub> in water was added to the reaction mixture to yield a dark purple–brown solid. This was filtered and the solid washed with water before being dried. The crude product was purified by silica column (19 : 1 : 0.1 CH<sub>3</sub>CN/H<sub>2</sub>O/KNO<sub>3</sub> (sat. solution in water)), the fractions containing the solid combined, and the solution concentrated. A saturated solution of NH<sub>4</sub>PF<sub>6</sub> in water was added to yield the product as a dark purple solid (40 mg, 29%). δ<sub>H</sub> (CD<sub>3</sub>CN, 500 MHz) 9.02 (s, 1H, H5a), 9.02 (s, 1H, H5), 8.54 (d, <sup>3</sup>J<sub>H–H</sub> 2.5, 1H, H21a), 8.53 (d, <sup>3</sup>J<sub>H–H</sub> 2.5, 1H, H21), 8.42–8.38 (m, 4H, H19 and H19a), 8.33 (d, <sup>3</sup>J<sub>H–H</sub> 8.0, 2H, H27), 8.08 (d, <sup>3</sup>J<sub>H–H</sub> 2.5, 1H, H13a), 8.06 (d, <sup>3</sup>J<sub>H–H</sub> 2.5, 1H, H13), 8.03 (t, <sup>3</sup>J<sub>H–H</sub> 8.0, 1H, H20a), 8.02 (t, <sup>3</sup>J<sub>H–H</sub> 8.0, 1H, H20), 7.89–7.85 (m, 4H, H6 and H8 and H26), 7.75 (dt, <sup>3</sup>J<sub>H–H</sub> 7.8, <sup>4</sup>J<sub>H–H</sub> 1.4, 1H, H14a), 7.70 (dt, <sup>3</sup>J<sub>H–H</sub> 7.8, <sup>4</sup>J<sub>H–H</sub> 1.4, 1H, H14), 7.58 (d, <sup>3</sup>J<sub>H–H</sub> 4.9, 1H, H24a), 7.55 (d, <sup>3</sup>J<sub>H–H</sub> 4.9, 1H, H24), 7.50–7.47 (m, 4H, H16, H6a, and H8a), 7.36–7.33 (m, 4H, H25, H6a, and H8a), 7.23 (dd, <sup>3</sup>J<sub>H–H</sub> 6.5, <sup>4</sup>J<sub>H–H</sub> 1.5, 2H, H10), 6.99–6.97 (m, 4H, H15 and H7a), 6.82 (d, <sup>3</sup>J<sub>H–H</sub> 9.0, 2H, H2a), 6.81 (d, <sup>3</sup>J<sub>H–H</sub> 9.0, 2H, H2), 6.47 (d, <sup>3</sup>J<sub>H–H</sub> 1.5, 2H, H6 and H8), 6.25 (d, <sup>3</sup>J<sub>H–H</sub> 9.0, 2H, H3a), 6.22 (d, <sup>3</sup>J<sub>H–H</sub> 9.0, 2H, H3), 6.11 (t, <sup>3</sup>J<sub>H–H</sub> 1.5, 2H, H7). <sup>13</sup>C{<sup>1</sup>H} NMR (CD<sub>3</sub>CN, 125 MHz) 161.2 (C18, C22), 160.0 (C23), 159.8 (C17), 154.6 (C14), 153.4 (C27), 149.3 (C1), 149.2 (C4), 148.9 (C6a and C8a), 146.3 (C9), 146.1 (C6 and C8), 137.8 (C6a and C8a, C6 and C8, C25), 137.0 (C15), 134.7 (C20), 131.3 (C10), 129.1 (C11), 128.2 (C26), 128.1 (C3), 127.6 (C12), 127.4 (C16), 124.6 (C24), 123.9 (C13), 123.1 (C2, C19, C21), 109.2 (C7a), 108.8 (C7), 76.5 (C5). Anal. Calc. for C<sub>62</sub>H<sub>49</sub>Cl<sub>2</sub>F<sub>12</sub>N<sub>15</sub>P<sub>2</sub>Ru: C 47.52, H 3.15, N 13.41. Found: C 47.22, H 2.98, N 13.65%. *m/z* (ESI<sup>+</sup>, MeOH) 638.40 (100%); [M – 2PF<sub>6</sub>]<sup>2+</sup> requires 638.59.

*[Ru<sub>3</sub>Cl<sub>3</sub>(tpy)<sub>3</sub>(TPA-3bpm)](PF<sub>6</sub>)<sub>3</sub>*

Ru(tpy)Cl<sub>3</sub> (77.4 mg, 0.176 mmol) and TPA-3bpm (40.0 mg, 0.0585 mmol) were suspended in dry methanol (40.0 mL) and *N*-methylmorpholine (2.5 mL) was added. The dark purple suspension was heated at reflux under nitrogen for 22 h, then cooled to room temperature. A saturated solution of KPF<sub>6</sub> in water was added to the reaction mixture to yield a dark purple–brown solid. This was filtered and the solid washed with water before being dried. The crude product was purified by silica column (19 : 1 : 0.1 CH<sub>3</sub>CN/H<sub>2</sub>O/KNO<sub>3</sub> (sat. solution in water)), the fractions containing the solid combined, and the solution concentrated. A saturated solution of NH<sub>4</sub>PF<sub>6</sub> in water was added to yield the product as a dark purple solid (80.0 mg, 49 %).  $\delta_{\text{H}}$  (CD<sub>3</sub>CN, 500 MHz) 8.73 (d, <sup>3</sup>*J*<sub>H–H</sub> 8.5, 6H, H15 and H17), 8.49–8.40 (m, 6H, H9, H16), 8.34 (d, <sup>3</sup>*J*<sub>H–H</sub> 8.0, 3H, H23), 7.93–7.89 (m, 9H, H5, H10, H22), 7.81 (d, <sup>3</sup>*J*<sub>H–H</sub> 1.5, 6H, H6 and H8), 7.69–7.67 (m, 3H, H12), 7.38–7.36 (m, 3H, H11), 7.33 (d, <sup>3</sup>*J*<sub>H–H</sub> 1.5, 3H, H20), 7.15 (t, <sup>3</sup>*J*<sub>H–H</sub> 6.0, 3H, H21), 6.93 (d, <sup>3</sup>*J*<sub>H–H</sub> 8.0, 6H, H2 and H3), 6.51 (br s, 6H, H6 and H8), 6.40 (d, <sup>3</sup>*J*<sub>H–H</sub> 8.0, 6H, H2 and H3), 6.13 (t, <sup>3</sup>*J*<sub>H–H</sub> 1.5, 6H, H7). <sup>13</sup>C{<sup>1</sup>H} NMR (CD<sub>3</sub>CN, 125 MHz) 160.0 (C19), 158.9 (C14 and C18), 156.3 (C14 and C18), 154.6 (C13), 149.0 (C4), 146.3 (C6 and C8), 139.0 (C5), 137.9 (C6 and C8, C10, C22), 137.1 (C12), 131.0 (C1), 128.5 (C21), 128.4 (C11), 128.3 (C20), 125.5 (C2 and C3), 125.3 (C9, C23), 124.1 (C15 and C17), 124.0 (C23), 122.8 (C16), 109.3 (C2 and C3), 108.9 (C7), 76.4 (C5). Anal. Calc. for C<sub>84</sub>H<sub>66</sub>Cl<sub>3</sub>F<sub>18</sub>N<sub>22</sub>P<sub>3</sub>Ru<sub>3</sub>: C 45.28, H 2.99, N 13.83. Found: C 45.27, H 2.59, N 13.53 %. *m/z* (ESI<sup>+</sup>, MeOH) 597.47 (100 %); [M – 3PF<sub>6</sub>]<sup>3+</sup> requires 597.73.

### Physical Measurements

#### Mass Spectrometry

Low-resolution ESI mass spectra were acquired as a solution in acetonitrile or methanol with a 100- $\mu\text{L min}^{-1}$  flow rate on a Finnegan LCQ MS detector. Spectra were collected over the mass range *m/z* 50 to 2000. An ESI spray voltage of 5 kV was applied with a heated capillary temperature of 200°C and a nitrogen sheath gas pressure of 60 psi (413 kPa).

#### Infrared Spectroscopy (Diffuse Reflectance Infrared Fourier Transform Spectroscopy)

Fourier-transform (FT)-IR was performed on samples in a KBr matrix over the range 4000–400  $\text{cm}^{-1}$  on a Bruker Tensor 27 FT-IR spectrometer with a resolution of 4  $\text{cm}^{-1}$ .

#### Electrochemistry

Solution-state electrochemical measurements were performed using a Bioanalytical Systems BAS 100A electrochemical analyser. Argon was bubbled through the electrolyte solution (0.1 M [(*n*-C<sub>4</sub>H<sub>9</sub>)<sub>4</sub>N]PF<sub>6</sub> in either CH<sub>3</sub>CN or CH<sub>2</sub>Cl<sub>2</sub>) containing a small sample of the compound of interest before the start of the experiment. The cyclic voltammograms (CVs) were recorded using a glassy carbon working electrode (1.5-mm diameter), a platinum wire auxiliary electrode, and an Ag/Ag<sup>+</sup> wire quasi-reference electrode. Ferrocene was added as an

internal standard on completion of each experiment. All potentials are quoted in volts versus Fc<sup>+</sup>/Fc.

#### UV-Vis-NIR Spectroelectrochemistry

Solution-state UV-vis-NIR spectroelectrochemistry over the range of 3500–35000  $\text{cm}^{-1}$  was performed using a Cary5000 spectrophotometer interfaced to Varian *WinUV* software. In the solution state, the absorption spectra of the electrogenerated species were obtained in situ by the use of an optically semi-transparent thin-layer electrosynthetic (OSTLE) cell, path length 0.65 mm, mounted in the path of the beam of the spectrophotometer. Solutions for the spectroelectrochemical experiment contained 0.1 M [(*n*-C<sub>4</sub>H<sub>9</sub>)<sub>4</sub>N]PF<sub>6</sub>/CH<sub>2</sub>Cl<sub>2</sub> or [(*n*-C<sub>4</sub>H<sub>9</sub>)<sub>4</sub>N]PF<sub>6</sub>/CH<sub>3</sub>CN supporting electrolyte and ~1 mM of the compound. Appropriate potentials were applied by using an eDAQ e-corder 410 potentiostat and the current was carefully monitored throughout the electrolysis. By this method, the electrogenerated species were obtained in situ, and their absorption spectra were recorded at regular intervals throughout the electrolysis.

#### EPR Spectroelectrochemistry

The procedure and cell set up used were as previously described.<sup>[41]</sup> A three-electrode assembly based on simple narrow wires (A–M Systems) as electrodes where Teflon-coated platinum (0.20 and 0.13 mm coated and uncoated diameters respectively) and silver wires (0.18 and 0.13 mm coated and uncoated diameters respectively) were used for the working and quasi-reference electrodes respectively, and a naked platinum wire (0.125 mm) for the counter electrode. The bottom 1 cm of the Teflon-coated wires was stripped (using an Eraser International Ltd RT2S fine wire stripper). The working electrode was positioned lowest such that the redox product of interest was generated at the bottom of the tube and well separated from the counter electrode. The electrodes were soldered to a narrow three-core microphone wire. The cell used was made by flame-sealing the tip of a glass pipette. The potential was controlled with a portable  $\mu\text{Autolab II}$  potentiostat and the EPR spectra obtained using an EMX Micro X-band EPR spectrometer with 1.0-T electromagnet.

#### Solution-State Fluorescence Spectroscopy

Fluorescence data were collected on a Cary Varian Eclipse fluorescence spectrophotometer. Excitation wavelengths were determined by UV-vis-NIR spectra, and maximum wavelengths deduced from emission–excitation spectra. The scan rate used for all measurements was 120  $\text{nm min}^{-1}$  with a 1-nm data interval. The fluorescence spectrum of the species of interest was obtained from a solution of the compound in acetone or acetonitrile in a quartz cuvette (1 × 1 × 1 cm) with excitation at 380 nm, the emission spectrum obtained from 400 to 750 nm, and slit widths of 2.5 mm, which were used for both excitation and emission.

#### Crystallography

*TPA-2bpm*.<sup>†</sup> A colourless block-like crystal was mounted on a SuperNova Dual Atlas diffractometer employing

<sup>†</sup>Formula C<sub>32</sub>H<sub>27</sub>N<sub>9</sub>, *M* 537.62, triclinic, *P*-1 space group (#02), *a* 9.9607(3), *b* 12.2145(3), *c* 12.9010(4) Å;  $\alpha$  110.727(3),  $\beta$  102.826(2),  $\gamma$  101.316(2)°; *V* 1364.85(7) Å<sup>3</sup>; *D<sub>c</sub>* 1.308 g cm<sup>-3</sup>; *Z* 2; crystal size 0.188 by 0.144 by 0.1 mm; colour: colourless; habit: block; temperature 150(2) K;  $\lambda$ (CuK $\alpha$ ) 1.54178 Å;  $\mu$ (CuK $\alpha$ ) 0.652 mm<sup>-1</sup>; *T*(CrysAlisPro, Agilent Technologies)<sub>min,max</sub> 0.93508, 1.00000;  $2\theta_{\text{max}}$  151.82; *hkl* range –12 12, –15 14, –16 16; *N* 24161, *N*<sub>ind</sub> 5651 (*R*<sub>merge</sub> 0.0196), *N*<sub>obs</sub> 5022(1 > 2 $\sigma$ (*I*)), *N*<sub>var</sub> 370; residuals *R*<sub>1</sub>(*F*) 0.0557, *wR*<sub>2</sub>(*F*<sup>2</sup>) 0.1369, GoF(all) 1.076, *D<sub>r</sub>*<sub>min,max</sub> –0.508, 0.570 e<sup>-</sup> Å<sup>-3</sup>. *R*<sub>1</sub> =  $\sum ||F_o| - |F_c|| / \sum |F_o|$  for *F*<sub>o</sub> > 2 $\sigma$ (*F*<sub>o</sub>); *wR*<sub>2</sub> =  $(\sum w(F_o^2 - F_c^2)^2 / \sum w(F_c^2)^2)^{1/2}$  all reflections  $w = 1/[ \sigma^2(F_o^2) + (0.0452P)^2 + 0.9594P ]$  where  $P = (F_o^2 + 2F_c^2)/3$ .

monochromated CuK $\alpha$  radiation generated from a sealed X-ray tube. Cell constants were obtained from a least-squares refinement against 14006 reflections located between 7.66 and 151.41° 2 $\theta$ . Data were collected at 150(2) K with  $\psi$  scans to 151.84° 2 $\theta$ . The data processing was undertaken with *CrysAlis Pro*<sup>[42]</sup> and subsequent computations were carried out with *WinGX*.<sup>[43]</sup> A multiscan absorption correction was applied<sup>[42]</sup> to the data.

The structure was solved in the triclinic space group *P*-1 (#2) by direct methods with *SHELXT*,<sup>[44]</sup> and extended and refined with *SHELXL-2014/7*.<sup>[45]</sup> The non-hydrogen atoms in the asymmetric unit were modelled with anisotropic displacement parameters. A riding atom model with group displacement parameters was used for the hydrogen atoms.

*TPA-3bpm*.<sup>‡</sup> A colourless plate crystal was coated in a thin film of Paratone-*N* oil before being mounted on a diffractometer with a ADSC Quantum 210r detector employing monochromated synchrotron radiation generated from the MX1 Beamline at the Australian Synchrotron in a stream of nitrogen at 100 K where the *Blu-Ice* graphical interface was used.<sup>[46]</sup> The data were reduced using the *XDS* package.<sup>[47]</sup> Cell constants were obtained from a least-squares refinement against 32066 reflections located between 2.80 and 64.00° 2 $\theta$ . Data were collected at 100(2) K with  $\psi$  scans to 54.97° 2 $\theta$ . Subsequent computations were carried out with *WinGX*.<sup>[43]</sup>

The structure was solved in the hexagonal space group *P*6<sub>3</sub>/m (#176) by direct methods with *SHELXT*,<sup>[44]</sup> and extended and refined with *SHELXL-2014/6*.<sup>[45]</sup> The non-hydrogen atoms in the asymmetric unit were modelled with anisotropic displacement parameters. A riding atom model with group displacement parameters was used for the hydrogen atoms.

## Supplementary Material

Characterization, electrochemistry, UV-vis-NIR spectro-electrochemistry, EPR spectroelectrochemistry, and fluorescence data are available on the Journal's website.

## Acknowledgement

We gratefully acknowledge support from the Australian Research Council and the Engineering and Physical Sciences Research Council UK National Electron Paramagnetic Resonance Service at the University of Manchester. The crystal structure of TPA-3bpm was obtained using the MX1 beamline at the Australian Synchrotron, Victoria, Australia.

## References

- [1] J. J. Concepcion, J. W. Jurss, M. K. Brennaman, P. G. Hoertz, A. O. T. Patrocino, N. Y. Murakami Iha, J. L. Templeton, T. J. Meyer, *Acc. Chem. Res.* **2009**, *42*, 1954. doi:10.1021/AR9001526
- [2] P. R. Andres, U. S. Schubert, *Adv. Mater.* **2004**, *16*, 1043. doi:10.1002/ADMA.200306518
- [3] A. O. Adeloye, P. A. Ajibade, *Molecules* **2014**, *19*, 12421.
- [4] L. Hammarström, O. Johansson, *Coord. Chem. Rev.* **2010**, *254*, 2546. doi:10.1016/J.CCR.2010.01.006
- [5] R. Sakamoto, S. Katagiri, H. Maeda, H. Nishihara, *Coord. Chem. Rev.* **2013**, *257*, 1493. doi:10.1016/J.CCR.2012.08.025
- [6] R. Shunmugam, G. J. Gabriel, K. A. Aamer, G. N. Tew, *Macromol. Rapid Commun.* **2010**, *31*, 784. doi:10.1002/MARC.200900869
- [7] A. Winter, S. Hoepfener, G. R. Newkome, U. S. Schubert, *Adv. Mater.* **2011**, *23*, 3484. doi:10.1002/ADMA.201101251
- [8] A. Wild, A. Winter, F. Schlutter, U. S. Schubert, *Chem. Soc. Rev.* **2011**, *40*, 1459. doi:10.1039/C0CS00074D
- [9] A. Winter, G. R. Newkome, U. S. Schubert, *ChemCatChem* **2011**, *3*, 1384. doi:10.1002/CCTC.201100118
- [10] J. Choi, H. M. Nguyen, S. Yoon, N. Kim, J.-W. Oh, F. S. Kim, *Mol. Cryst. Liq. Cryst.* **2014**, *600*, 22. doi:10.1080/15421406.2014.936525
- [11] P. Hrobárik, V. Hrobáriková, I. Sigmundová, P. Zahradník, M. Fakis, I. Polyzos, P. Persephonis, *J. Org. Chem.* **2011**, *76*, 8726. doi:10.1021/JO201411T
- [12] C.-J. Yao, Y.-W. Zhong, J. Yao, *Inorg. Chem.* **2013**, *52*, 10000. doi:10.1021/IC401288G
- [13] C. Lambert, G. Nöll, *Angew. Chem. Int. Ed.* **1998**, *37*, 2107. doi:10.1002/(SICI)1521-3773(19980817)37:15<2107::AID-ANIE2107>3.0.CO;2-H
- [14] C. Lambert, G. Nöll, *J. Am. Chem. Soc.* **1999**, *121*, 8434. doi:10.1021/JA991264S
- [15] C. Lambert, G. Nöll, *Synth. Met.* **2003**, *139*, 57. doi:10.1016/S0379-6779(02)01250-X
- [16] C. Lambert, S. Amthor, J. Schelter, *J. Phys. Chem. A* **2004**, *108*, 6474. doi:10.1021/JP048449S
- [17] S. Amthor, C. Lambert, *J. Phys. Chem. A* **2006**, *110*, 1177. doi:10.1021/JP0550309
- [18] C. Lambert, C. Risko, V. Coropceanu, J. Schelter, S. Amthor, N. E. Gruhn, J. C. Durivage, J.-L. Brédas, *J. Am. Chem. Soc.* **2005**, *127*, 8508. doi:10.1021/JA0512172
- [19] A. Heckmann, C. Lambert, *Angew. Chem. Int. Ed.* **2012**, *51*, 326. doi:10.1002/ANIE.201100944
- [20] M. Parthey, M. Kaupp, *Chem. Soc. Rev.* **2014**, *43*, 5067. doi:10.1039/C3CS60481K
- [21] D. M. D'Alessandro, F. R. Keene, *Chem. Soc. Rev.* **2006**, *35*, 424.
- [22] D. M. D'Alessandro, F. R. Keene, *Chem. Rev.* **2006**, *106*, 2270. doi:10.1021/CR050010O
- [23] P. J. Low, *Dalton Trans.* **2005**, 2821. doi:10.1039/B506017F
- [24] C. A. Bignozzi, R. Argazzi, R. Boaretto, E. Busatto, S. Carli, F. Ronconi, S. Caramori, *Coord. Chem. Rev.* **2013**, *257*, 1472. doi:10.1016/J.CCR.2012.09.008
- [25] A. Orbelli Biroli, F. Tessore, M. Pizzotti, C. Biaggi, R. Ugo, S. Caramori, A. Aliprandi, C. A. Bignozzi, F. De Angelis, G. Giorgi, E. Licandro, E. Longhi, *J. Phys. Chem. C* **2011**, *115*, 23170. doi:10.1021/JP2030363
- [26] A. Yella, H.-W. Lee, H. N. Tsao, C. Yi, A. K. Chandiran, M. K. Nazeeruddin, E. W.-G. Diao, C.-Y. Yeh, S. M. Zakeeruddin, M. Grätzel, *Science* **2011**, *334*, 629. doi:10.1126/SCIENCE.1209688
- [27] M. Thelakkat, *Macromol. Mater. Eng.* **2002**, *287*, 442. doi:10.1002/1439-2054(20020701)287:7<442::AID-MAME442>3.0.CO;2-H
- [28] T. Lana-Villarreal, J. M. Campiña, N. Guijarro, R. Gómez, *Phys. Chem. Chem. Phys.* **2011**, *13*, 4013. doi:10.1039/C0CP01818J
- [29] A. Petr, C. Kvarnström, L. Dunsch, A. Ivaska, *Synth. Met.* **2000**, *108*, 245. doi:10.1016/S0379-6779(99)00137-X
- [30] S. Amthor, B. Noller, C. Lambert, *Chem. Phys.* **2005**, *316*, 141. doi:10.1016/J.CHEMPHYS.2005.05.009
- [31] N. S. Hush, *Electrochim. Acta* **1968**, *13*, 1005. doi:10.1016/0013-4686(68)80032-5
- [32] G. C. Allen, N. S. Hush, *Inorg. Chem.* **1967**, *6*, 4. doi:10.1021/IC50047A002
- [33] M. B. Robin, P. Day, in *Advances in Inorganic Chemistry and Radiochemistry* (Eds H. J. Emeléus, A. G. Sharpe) **1968**, Vol. 10, pp. 247–422 (Academic Press: New York, NY).

<sup>‡</sup>Formula C<sub>39</sub>H<sub>33</sub>N<sub>13</sub>O<sub>1.62</sub>, *M* 709.65, hexagonal, *P*6<sub>3</sub>/m space group (#176), *a* 11.903(2), *b* 11.903(2), *c* 14.466(3) Å;  $\gamma$  120°; *V* 1775.0(7) Å<sup>3</sup>; *D*<sub>c</sub> 1.328 g cm<sup>-3</sup>; *Z* 2; crystal size 0.10 by 0.10 by 0.06 mm; colour: colourless; habit: plate; temperature 100(1) K;  $\lambda$ (synchrotron) 0.7109 Å;  $\mu$ (synchrotron) 0.087 mm<sup>-1</sup>; T(XDS (Kabsch, 1993))<sub>min,max</sub> 0.6635, 0.7463, 2 $\theta$ <sub>max</sub> 54.97; *hkl* range -15 15, -15 15, -18 18; *N* 27876, *N*<sub>ind</sub> 1410 (*R*<sub>merge</sub> 0.0701), *N*<sub>obs</sub> 1286 (*I* > 2 $\sigma$ (*I*)), *N*<sub>var</sub> 152, residuals *R*<sub>1</sub>(*F*) 0.0761, *wR*<sub>2</sub>(*F*<sup>2</sup>) 0.1801, GoF(all) 1.124,  $\Delta\rho$ <sub>min,max</sub> -0.186, 0.189 e<sup>-</sup> Å<sup>-3</sup>. *R*<sub>1</sub> =  $\sum||F_o| - |F_c|| / \sum|F_o|$  for *F*<sub>o</sub> > 2 $\sigma$ (*F*<sub>o</sub>); *wR*<sub>2</sub> =  $(\sum w(F_o^2 - F_c^2)^2 / \sum w(F_c^2)^2)^{1/2}$  all reflections *w* = 1/[ $\sigma^2(F_o^2) + (0.0560P)^2 + 1.1154P$ ] where *P* = (*F*<sub>o</sub><sup>2</sup> + 2*F*<sub>c</sub><sup>2</sup>)/3.

- [34] D. R. Kattnig, B. Mladenova, G. Grampp, C. Kaiser, A. Heckmann, C. Lambert, *J. Phys. Chem. C* **2009**, *113*, 2983. doi:10.1021/JP8107705
- [35] G. Lemercier, A. Bonne, M. Four, L. M. Lawson-Daku, *C. R. Chim.* **2008**, *11*, 709. doi:10.1016/J.CRCI.2007.11.012
- [36] C. Hua, D. M. D'Alessandro, *CrystEngComm* **2014**, *16*, 6331. doi:10.1039/C3CE42603C
- [37] F. J. Rizzuto, T. B. Faust, B. Chan, C. Hua, D. M. D'Alessandro, C. J. Kepert, *Chem. – Eur. J.* **2014**, *20*, 17597. doi:10.1002/CHEM.201405089
- [38] Y. Nakano, T. Yagyu, T. Hirayama, A. Ito, K. Tanaka, *Polyhedron* **2005**, *24*, 2141. doi:10.1016/J.POLY.2005.03.031
- [39] D. Hvasanov, A. F. Mason, D. C. Goldstein, M. Bhadbhade, P. Thordarson, *Org. Biomol. Chem.* **2013**, *11*, 4602. doi:10.1039/C3OB40620B
- [40] B. P. Sullivan, J. M. Calvert, T. J. Meyer, *Inorg. Chem.* **1980**, *19*, 1404. doi:10.1021/IC50207A066
- [41] Y. Liu, J.-R. Li, W. M. Verdegaal, T.-F. Liu, H.-C. Zhou, *Chem. – Eur. J.* **2013**, *19*, 5637. doi:10.1002/CHEM.201203297
- [42] *CrysAlis PRO 2014* (Agilent Technologies Ltd: Yarnton, UK).
- [43] L. Farrugia, *J. Appl. Cryst.* **1999**, *32*, 837. doi:10.1107/S0021889899006020
- [44] G. M. Sheldrick, *Acta Crystallogr. Sect. A* **2015**, *A71*, 3. doi:10.1107/S2053273314026370
- [45] G. M. Sheldrick, *SHELXTL Reference Manual: Version 5 1996* (Analytical X-ray Instruments Inc.: Madison, WI).
- [46] T. M. McPhillips, S. E. McPhillips, H.-J. Chiu, A. E. Cohen, A. M. Deacon, P. J. Ellis, E. Garman, A. Gonzalez, N. K. Sauter, R. P. Phizackerley, S. M. Soltis, P. Kuhn, *J. Synchrotron Radiat.* **2002**, *9*, 401. doi:10.1107/S0909049502015170
- [47] W. Kabsch, *Acta Crystallogr. Sect. D* **2010**, *66*, 125. doi:10.1107/S0907444909047337